Journal of Hazardous Materials 192 (2011) 1539–1547

Contents lists available at ScienceDirect

Journal of Hazardous Materials

journal homepage: www.elsevier.com/locate/jhazmat

Surface engineered magnetic nanoparticles for removal of toxic metal ions and bacterial pathogens

Sarika Singh, K.C. Barick[1], D. Bahadur*

Department of Metallurgical Engineering and Materials Science, Indian Institute of Technology Bombay, Mumbai 400076, India

ARTICLE INFO

Article history:
Received 15 February 2011
Received in revised form 27 June 2011
Accepted 27 June 2011
Available online 1 July 2011

Keywords:
Nanoparticles
Magnetic
Surface functionalization
Toxic metal ions
Bacterial pathogens
Waste-water

ABSTRACT

Surface engineered magnetic nanoparticles (Fe_3O_4) were synthesized by facile soft-chemical approaches. XRD and TEM analyses reveal the formation of single-phase Fe_3O_4 inverse spinel nanostructures. The functionalization of Fe_3O_4 nanoparticles with carboxyl (succinic acid), amine (ethylenediamine) and thiol (2,3-dimercaptosuccinic acid) were evident from FTIR spectra, elemental analysis and zeta-potential measurements. From TEM micrographs, it has been observed that nanoparticles of average sizes about 10 and 6 nm are formed in carboxyl and thiol functionalized Fe_3O_4, respectively. However, each amine functionalized Fe_3O_4 is of size ~40 nm comprising numerous nanoparticles of average diameter 6 nm. These nanoparticles show superparamagnetic behavior at room temperature with strong field dependent magnetic responsivity. We have explored the efficiency of these nanoparticles for removal of toxic metal ions (Cr^{3+}, Co^{2+}, Ni^{2+}, Cu^{2+}, Cd^{2+}, Pb^{2+} and As^{3+}) and bacterial pathogens (*Escherichia coli*) from water. Depending upon the surface functionality (COOH, NH_2 or SH), magnetic nanoadsorbents capture metal ions either by forming chelate complexes or ion exchange process or electrostatic interaction. It has been observed that the capture efficiency of bacteria is strongly dependent on the concentration of nanoadsorbents and their inoculation time. Furthermore, these nanoadsorbents can be used as highly efficient separable and reusable materials for removal of toxic metal ions.

1. Introduction

Development of novel and cost-effective nanomaterials for environmental remediation, pollution detection and many others has attracted considerable attention in recent past. Contamination of water with toxic metal ions (Cr^{3+}, Ni^{2+}, Co^{2+}, Cu^{2+}, Cd^{2+}, Ag^{+}, Hg^{2+}, Pb^{2+} and As^{3+}) and microorganisms (*Escherichia coli* (*E. coli*), *Sarcina lutea* (*S. lutea*) and *Staphylococcus aureus* (*S. aureus*)) is becoming a severe environmental and public health problem [1,2]. In order to achieve environmental detoxification, various techniques like adsorption, precipitation, ion exchange, reverse osmosis, electrochemical treatments, membrane filtration, evaporation, flotation, oxidation and biosorption processes are extensively used [3–5]. Among these, adsorption is a conventional but efficient technique to remove toxic metal ions and bacterial pathogens from water. Numerous adsorbents have been developed for the purification of waste-water [6–8]. In most cases, these adsorbents are highly porous materials, providing ample surface area for adsorption. However, the existence of intraparticle diffusion may lead to the decrease in available space and adsorption capacity. Thus, the development of efficient biocompatible adsorbent having large surface area, active surface sites and low intraparticle diffusion rate is of great significance in practical engineering applications.

Recently, magnetic nanoparticles (MNP) such as Fe_3O_4 and γ-Fe_2O_3 have been investigated to resolve various environmental problems, such as removing toxic metal ions and radioactive elements, capturing of microbial pathogens and organic dyes, accelerating the coagulation of sewage, and remediation of contaminated soils [9–13]. The magnetic nanoparticles possess high surface area and optimal magnetic properties, which lead to high adsorption efficiency, high removal rate of contaminants, and easy and rapid separation of adsorbent from solution via magnetic field. The magnetic nanoparticles can be reusable after magnetic separation by removing the adsorbed toxic contaminants [10]. Furthermore, magnetic nanoparticles functionalized with biorecognition molecules such as antibody, bioprotein and carbohydrates [14,15] or biocompatible organic/inorganic molecules [16,17], polymers and dendrimers [17–19] are more effective since the free functional groups present on the surface provide large number of active sites as well as aqueous stability, which is necessary for the successful adsorption of toxic metal ions and bacterial pathogens [20,21]. In order to achieve this, new and effective aqueous stabilized surface engineered/surface functionalized magnetic nanoparticles with low regeneration cost are needed. However, the

* Corresponding author. Tel.: +91 22 2576 7632; fax: +91 22 2572 3480.
E-mail address: dhirenb@iitb.ac.in (D. Bahadur).
[1] Present address: Chemistry Division, Bhabha Atomic Research Centre, Mumbai 400085, India.

0304-3894/$ – see front matter © 2011 Elsevier B.V. All rights reserved.
doi:10.1016/j.jhazmat.2011.06.074

research in this area is in its nascent stage and detail investigations are required to establish the large scale purification of water in real life.

Herein, we have prepared aqueous stable carboxyl (succinic acid), amine (ethylenediamine) and thiol (2,3-dimercaptosuccinic acid) functionalized Fe_3O_4 MNP and investigated their efficiency for the simultaneous removal of multiple toxic metal ions (Cr^{3+}, Co^{2+}, Ni^{2+}, Cu^{2+}, Cd^{2+}, Pb^{2+} and As^{3+}) as well as bacterial pathogens (*E. coli*) from water. In addition, we have also investigated the possibility to reuse these magnetic nanoadsorbents in succeeding cycles for removal of toxic metal ions.

2. Experimental

2.1. Preparation and characterization of surface engineered magnetic nanoparticles

Three different synthesis methods were used in preparing surface engineered Fe_3O_4 MNP. The aqueous stable carboxyl functionalized Fe_3O_4 magnetic nanoparticles (carboxyl MNP) were obtained by co-precipitation method. In a typical synthesis, 5.406 g of $FeCl_3$, $6H_2O$ and 1.988 g of $FeCl_2$, $6H_2O$ were dissolved in 80 ml of water in a round bottom flask and temperature was slowly increased to 70 °C in refluxing condition under nitrogen atmosphere with constant mechanical stirring at 1000 rpm. The temperature was maintained at 70 °C for 30 min and then 20 ml of 25% ammonia solution was added instantaneously to the reaction mixture, and kept for another 30 min at 70 °C. Then, 4 ml aqueous solution (0.3 gm/ml) of succinic acid (SA) was added and temperature was slowly raised up to 90 °C under reflux and reacted for 60 min with continuous stirring. The obtained black coloured precipitates were then thoroughly rinsed with water and separated from the supernatant using a permanent magnet.

The aqueous stable amine functionalized Fe_3O_4 magnetic nanoparticles (amine MNP) were obtained by a single step process through thermal decomposition of Fe-chloride precursors in presence of sodium acetate and ethylenediamine (EDA) in ethylene glycol medium as discussed elsewhere [22]. The aqueous stable thiol functionalized Fe_3O_4 magnetic nanoparticles (thiol MNP) were prepared by a two step process. The Fe_3O_4 nanoparticles were first prepared by thermal decomposition of iron (III) acetylacetonate in presence of dodecylamine, lauric acid and 1,2-hexadecanediol surfactants in benzyl ether medium at elevated temperature as discussed elsewhere [16]. These nanoparticles are coated with lauric acid and dodecylamine, and thus hydrophobic in nature. In order to make them hydrophilic and biocompatible, thiol groups (DMSA) were introduced onto the surface of nanoparticles through a well-established ligand exchange process [16]. The detail experimental procedures for preparation of amine and thiol MNP are described in Supplementary data.

X-ray diffraction (XRD) patterns were recorded on a PANalytical's X'Pert PRO diffractometer with Cu Kα radiation. The infrared spectra (3000–500 cm^{-1}) were recorded on a Fourier transform infrared spectrometer (Magna 550 FTIR, Nicolet Instruments Corp.). The transmission electron micrographs were taken by Philips CM 200 TEM. The elemental analyses were performed on Thermo Fennigan FLASH EA 1112 series CHNS(O) analyzer. The hydrodynamic diameter and electrokinetic behavior (zeta-potential) were determined by dynamic light scattering (DLS) and zeta potential analyzer, respectively (Brookhaven Instruments Corp.). The field and temperature dependent magnetization measurements were carried out by vibrating sample magnetometer (VSM-7410, Lake Shore). The temperature dependendent magnetization measurements were carried out at a field of 100 Oe to determine the Curie temperature (T_C). The scanning electron micrographs were taken by Hitachi S-3400N SEM. The elemental analysis and spectral mapping were carried out by using energy dispersive spectroscopy (EDS) facility of Hitachi S-3400N SEM.

2.2. Removal of toxic metal ions by surface engineered magnetic nanoparticles

In order to investigate the pH dependent removal efficiency of toxic metal ions by surface functionalized Fe_3O_4 nanoparticles, adsorption experiments were conducted by mixing 40 ml of waste-water containing different toxic metal ions (10.17 mg/L Cr^{3+}, 15.75 mg/L Co^{2+}, 25.13 mg/L Ni^{2+}, 23.83 mg/L Cu^{2+}, 47.8 mg/L Cd^{2+}, 42.0 mg/L Pb^{2+} and 19.6 mg/L As^{3+}) with 50 mg of magnetic nanoadsorbents (carboxyl MNP, amine MNP or thiol MNP) at different pH (2–12). The pH of the reaction mixtures was adjusted with aqueous solution of HCl and NaOH. The above mixture was kept under continuous shaking for 24 h at room temperature (30 °C). Further, the adsorption experiments were carried out at pH 6 with varying concentration of nanoadsorbent (50, 5 and 0.5 mg of amine MNP in 40 ml of waste-water keeping all other parameters constant, i.e. solid/liquid (S/L) ratio in the range of 10^{-3}–10^{-5} g/ml) to investigate the effect S/L ratio on adsorption efficiency metal ions.

For adsorption kinetic studies, 50 mg of nanoadsorbents were added to 40 ml of prepared waste-water as described above. The reaction mixtures were kept under continuous shaking for different contact time at room temperature. The surface functionalized Fe_3O_4 nanoparticles with adsorbed metal ions were separated from the mixture by a permanent magnet. The concentrations of metal ions were measured by inductively coupled plasma-atomic emission spectrometer (ICP-AES, 8440 Plasmalab, Labtam). The adsorption experiments were performed in triplicates and the averaged values are reported here. The removal efficiency (%) and equilibrium adsorbed concentration, q (mg/g) of metal ions were calculated as follows:

$$\text{Removal efficiency } (\%) = \frac{(C_o - C_t)}{C_o} \times 100 \quad (1)$$

$$q = (C_o - C_t) \times \frac{V}{M} \quad (2)$$

where C_o and C_t are the initial and residual concentration of metal ions (mg/L) in aqueous solution, V is the total volume of solution (L) and M is the adsorbent mass (g).

Further to examine the feasibility of recycling magnetic nanoadsorbents, desorption studies were performed at weak acidic medium. In the desorption process, 50 mg of used magnetic nanoadsorbents (amine MNP with adsorbed metal ions at pH 8) were dispersed into 10 mL of 0.1 M HCl by ultrasonication for 15 min. The above mixture was further kept for 24 h at room temperature for desorption of metal ions. The magnetic nanoadsorbents were thoroughly gathered once again by an external magnet and washed with Milli Q water several times and reconditioned for adsorption in succeeding cycles. The regenerated magnetic nanoadsorbents (amine MNP) were reused for adsorption of metal ions as described above at pH 8. The desorption ratio of metal ions was determined using the following equation:

$$\text{Desorption ratio } (\%) = \left(\frac{\text{Amount of desorbed metal ion}}{\text{Amount of adsorbed metal ion}}\right) \times 100 \quad (3)$$

2.3. Capturing of bacteria by surface engineered magnetic nanoparticles

The ability of surface engineered MNP to capture bacterial pathogens was examined using *E. coli* BL-21 as a model microorganism. *E. coli* pathogens were thawed on ice for 15 min before being plated on an agar plate. The plate was dried before incubation for 16 h in a standard cell culture environment (5% CO_2, 37 °C).

A single colony of *E. coli* was selected using a loop and inoculated into centrifuge tubes containing 5 ml of Luria Broth (LB). Bacteria in centrifuge tubes were then incubated in cell culture environment under agitation at 250 rpm for another 12 h. At that point, the bacteria solution was diluted in LB to a desired optical density (0.1) at 600 nm (OD_{600}) using a UV–vis spectroscopy (GeneQuant 1300 Spectrophotometer).

The different concentrations of nanoadsorbents suspended in PBS (0.05, 0.5, 1.0 and 2.0 mg/ml) were then added into the tube containing bacterial solution, and the solution volume was fixed to 6 ml. A tube of bacteria without nanoadsorbents served as a control. The suspensions of nanoadsorbents were also added to tubes containing only LB at the same concentration as above and this served as a particle control. The solutions were incubated by a rotary shaker at 250 rpm for a specific period (12 h and 24 h), then an external magnet was used for magnetic separation. The supernatant was used to measure its OD_{600}. The capture efficiency of bacteria by nanoadsorbents was calculated from the decrease of turbidity relative to the reference samples. For safety considerations, all of the bacterial samples were placed in an autoclave at 120 °C for 20 min to kill bacteria before disposal and all glassware in contact with bacteria was sterilized before and after use.

3. Results and discussion

3.1. Structural/microstructural characterizations

XRD patterns of carboxyl MNP, amine MNP and thiol MNP (Fig. S1 of Supplementary data) reveal the formation of single-phase inverse spinel magnetite, Fe_3O_4 with lattice constant, $a = \sim 8.378$ Å, which is very close to the reported value (JCPDS Card No. 88-0315, $a = 8.375$ Å). From X-ray line broadening, the crystallite size of carboxyl MNP, amine MNP and thiol MNP are estimated around 10, 8 and 6 nm, respectively.

Fig. 1 shows TEM micrographs of (a) carboxyl MNP, (b) amine MNP and (c) thiol MNP. TEM micrographs clearly show the formation of roughly spherical nanoparticles of average size 10 nm ($\sigma < 10\%$) in carboxyl MNP and highly monodisperse well-spherical nanoparticles of average size 6 nm ($\sigma < 5\%$) in thiol MNP samples. However, amine MNP sample is well-defined, homogeneous with discrete morphology but porous in nature. Each amine MNP is of average size 40 nm ($\sigma < 10\%$) and made up of three-dimensionally spatially connected numerous nanocrystalites with an average diameter of about 6 nm. The possible mechanism for the formation of porous structure of amine MNP is presented elsewhere [16]. Furthermore, the electron diffraction patterns of surface engineered magnetic nanoparticles can be indexed to the highly crystalline reflections of cubic inverse spinel Fe_3O_4 structure, which is consistent with XRD result. A typical electron diffraction pattern of thiol MNP is shown in inset of Fig. 1(c).

Fig. 2 shows FTIR spectra of (a) SA and carboxyl MNP, (b) EDA and amine MNP, and (c) DMSA and thiol MNP with their band assignments. The vibrational bands for SA, EDA and DMSA are well resolved, but those of carboxyl, amine and thiol functionalized Fe_3O_4 are rather broad and few. The bands at 1690 and 1700 cm^{-1} could be assigned to C═O vibration (asymmetric stretching) of SA and DMSA, respectively, which shifts to a lower value for carboxyl and thiol MNP revealing the binding of these organic components to surface of Fe_3O_4 nanoparticles by chemisorptions of carboxylate ions [23]. Furthermore, the vibrational modes appearing at 1390 and 1400 cm^{-1} in carboxyl MNP and thiol MNP, respectively correspond to the symmetric stretching of COO^- group of SA and DMSA [23]. The vibrational modes attributed to the amine groups such as NH_2 scissoring at 1595 cm^{-1}, C—N stretching at 1320 cm^{-1} and NH wagging at 932 cm^{-1} are clearly observed in the FTIR spectrum

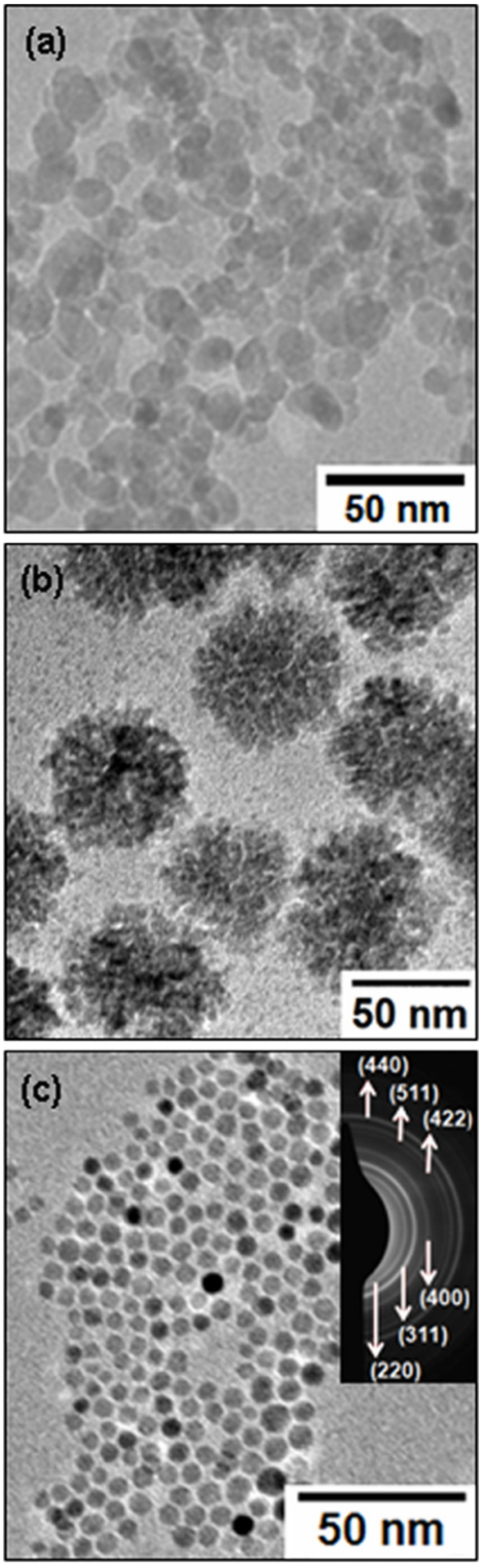

Fig. 1. TEM micrographs of (a) carboxyl MNP, (b) amine MNP and (c) thiol MNP. A typical electron diffraction pattern of thiol MNP is shown in inset of Fig. 1 (c).

of amine MNP with a slight shift in their band positions indicating the functionalization of Fe_3O_4 with EDA [22]. The strong IR band observed at around 588 cm^{-1} in carboxyl, amine and thiol MNP can be ascribed to the Fe—O stretching vibrational mode of Fe_3O_4. The band corresponding to SH group of DMSA is not clearly observed in

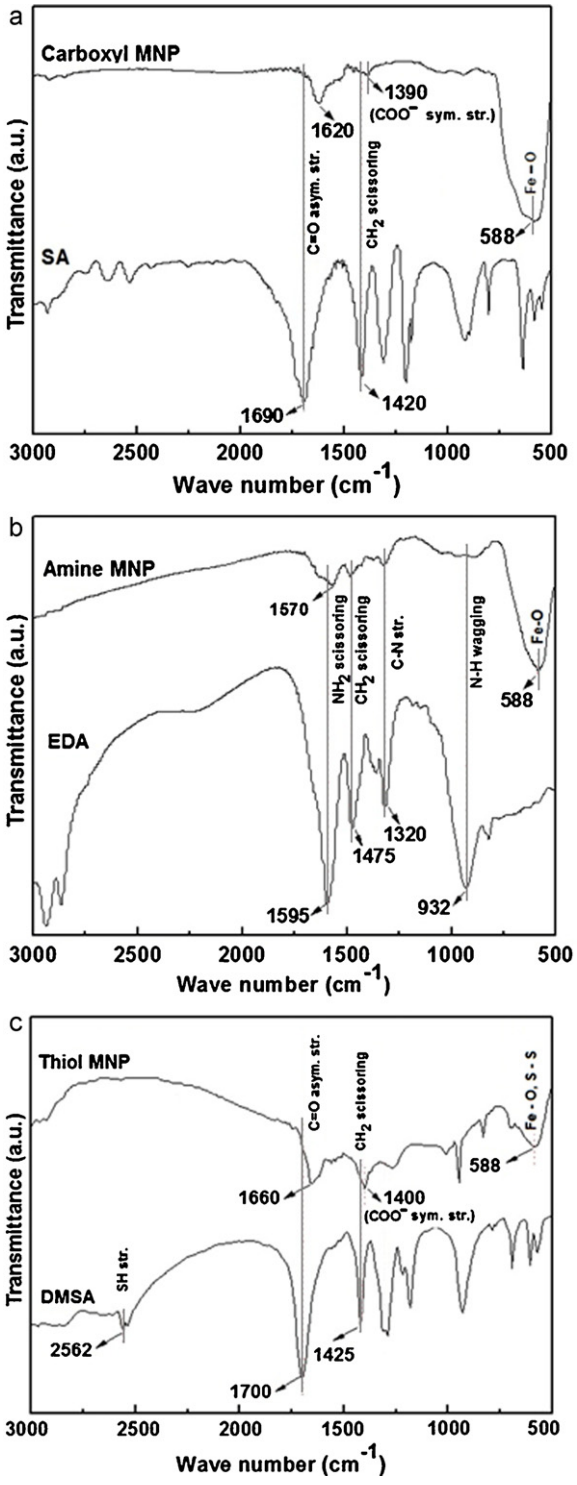

Fig. 2. FTIR spectra of (a) SA and carboxyl MNP, (b) EDA and amine MNP, and (c) DMSA and thiol MNP with their band assignments.

thiol MNP possibly due to the formation of disulfide (S—S) linkage which overlaps with the Fe—O vibration of Fe_3O_4 [24]. Furthermore, the elemental analysis of surface engineered nanoparticles indicates the presence of the respective organic components (carbon, hydrogen, nitrogen or sulfur) in the samples (Table S1 of Supplementary data). These results confirmed that Fe_3O_4 nanoparticles have been successfully functionalized with SA, EDA and DMSA during the course of synthesis.

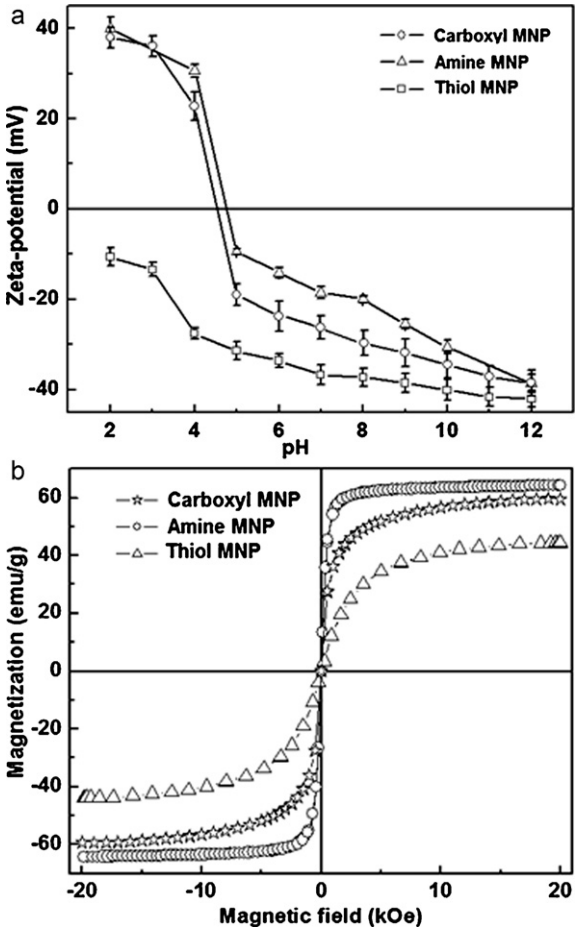

Fig. 3. (a) pH dependent zeta-potential and (b) field dependent magnetization plots of carboxyl MNP, amine MNP and thiol MNP at room temperature.

3.2. Electrokinetics and magnetic properties

Fig. 3 shows (a) pH dependent zeta-potential and (b) field dependent magnetization plots of carboxyl MNP, amine MNP and thiol MNP at room temperature. From Fig. 3(a), the pH of zero point charge (pH_{pzc}) of carboxyl MNP and amine MNP were found to be around 4.5 and 4.7, respectively whereas that of thiol MNP is not observed in measured pH range. Thus, the carboxyl MNP and amine MNP have positive surface charge at $pH < pH_{pzc}$ and negative surface charge at $pH > pH_{pzc}$. However, thiol MNP reveals negative surface charge in the pH range of 2–12. The difference in their charge properties may be attributed to the ionization of functional groups, such as —COOH, —NH_2 and —SH at different pH. It has been observed that the pH_{pzc} of Fe_3O_4 decreases upon binding of SA, EDA and DMSA onto the surface of Fe_3O_4 nanoparticles (pH_{pzc} of bare Fe_3O_4 nanoparticles is 6.7 [25]). Furthermore, DLS measurements (Fig. S2 of Supplementary data) indicate that these nanoparticles render aqueous colloidal suspension with mean hydrodynamic diameters (invariable change in polydispersity index) of about 25 nm, 90 nm and 17 nm ($\sigma < 5\%$) for carboxyl, amine and thiol MNP, respectively due to the presence of associated and hydrated organic layers [16]. Specifically, some of the carboxylate (incase of SA and DMSA) and amine (incase of EDA) groups strongly coordinate to iron cations on the Fe_3O_4 surface to form a robust coating, while uncoordinated carboxylate, amine and thiol groups extend into water medium, conferring a high degree of aqueous stability to Fe_3O_4 nanoparticles. In addition, the electrostatic repulsive force which may originate among the nanoparticles in aqueous suspension also plays an important role in their stabilization.

Magnetization measurements were mainly performed to investigate the use of these surface engineered nanoparticles as a magnetic nanoadsorbent in the magnetic separation. The field dependent magnetization plots of carboxyl MNP, amine MNP and thiol MNP (Fig. 3(b)) exhibit superparamagnetic behavior without magnetic hysteresis and remanence at room temperature. The maximum magnetizations of carboxyl MNP, amine MNP and thiol MNP were found to be 59.5, 64.3 and 43.2 emu/g, respectively at 20 kOe. Such magnetic properties mean that these surface engineered MNP have strong magnetic responsivity and can be separated easily from the solution with the help of an external magnetic force. Furthermore, the Curie temperature (T_C) of these magnetic nanoparticles was found to be 580 °C, which is in agreement with that reported for Fe_3O_4 whereas the T_C of γ-Fe_2O_3 is around 645 °C [16,26]. These results suggest that the phase formed is Fe_3O_4 rather than γ-Fe_2O_3.

3.3. Removal of toxic metal ions by surface engineered magnetic nanoparticles

Fig. 4 shows pH dependent removal efficiency of toxic metal ions by (a) carboxyl MNP, (b) amine MNP and (c) thiol MNP. It has been observed that the removal efficiency of metal ions (M^{n+} = Cr^{3+}, Co^{2+}, Ni^{2+}, Cu^{2+}, Cd^{2+}, Pb^{2+} and As^{3+}) is strongly dependent on pH of the solution. The extraction rates of Cr^{3+}, Co^{2+}, Ni^{2+}, Cu^{2+}, Cd^{2+} and Pb^{2+} ions gradually increase with increasing pH of the solution till extraction rates approach a plateau. The tabular representation of removal efficiency of metal ions is provided in Table S2 Supplementary data. Almost 100% removal of Cr^{3+}, Co^{2+}, Ni^{2+}, Cu^{2+}, Cd^{2+} and Pb^{2+} ions from waste-water are obtained at higher pH (except As^{3+}). However, the optimal adsorption of As^{3+} was found to be about 91%, 95% and 97% by carboxyl, amine and thiol MNP, respectively at pH 8 (removal efficiency decreases above pH 8). This seems to be the pH range at which hydrolyzed forms of As^{3+} such as AsO_3^{3-} or $As(OH)_4^-$ appear (formed by reaction of As^{3+} with OH^- ions). Furthermore, the suppressed adsorption of metal ions at low pH implies that acid treatment is a feasible approach to regenerate these nanoadsorbents. In addition to the ICP-AES analysis, the adsorption of metal ions by surface engineered MNP was also evident from the SEM-EDS analyses of metal ions adsorbed nanoadsorbents (Fig. S3 of Supplementary data shows a typical SEM-EDS analysis of thiol MNP with adsorbed metal ions in aqueous medium at pH 8). The removal efficiency of metal ions by surface engineered MNP was also found to be dependent on the concentration of nanoadsorbents. The adsorption experiments carried out with varying concentration of nanoadsorbents (50, 5 and 0.5 mg in 40 ml of waste-water, i.e. S/L ratio in the range of 10^{-3}–10^{-5} g/ml) revealed that removal efficiency increases with increasing the concentration of nanoadsorbents (Fig. S4 of Supplementary data shows a typical removal efficiency plot of metal ions with different concentrations of amine MNP at pH 6). This is obvious as the availability of active surface sites for adsorption of metal ions increases with increasing the concentration of nanoadsorbents [27]. Thus, the efficiency of simultaneous adsorption of metal ions can be explained on the basis of surface functionality, competitive affinity of metal ions for Fe_3O_4, amount of surface charge and availability of active surface sites on Fe_3O_4 nanoparticles. The schematic representations of possible mechanism for adsorption of metal ions by (a) carboxyl MNP, (b) amine MNP and (c) thiol MNP are shown in Scheme 1.

In case of carboxyl MNP, the negatively charged carboxylate ions (COO^-) have strong coordinative affinity towards metal ions. These carboxylate ions capture the toxic metal ions by forming chelate complexes for pH > pH_{pzc} (Scheme 1(a)). The ability of surface complexation of carboxyl MNP with metal ions increases with increasing pH of the solution which leads to almost 100% removal of all analyzed metal ions (except As^{3+}) at higher pH. The enhanced

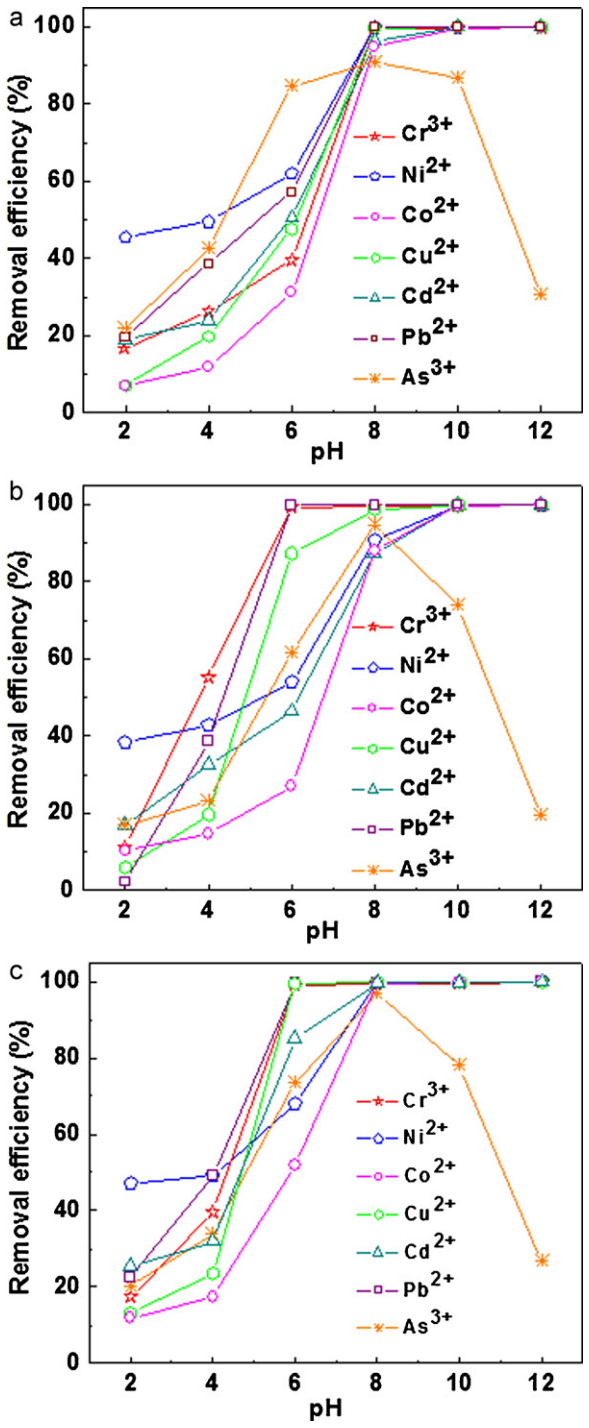

Fig. 4. pH dependent removal efficiency of toxic metal ions by (a) carboxyl MNP, (b) amine MNP and (c) thiol MNP.

chelation tendency of carboxylate ions at higher pH is expected as at lower pH, the chelation sites were occupied with H^+ (chelation sites are neutral, i.e. —COOH) and they were released at higher pH originating the desired chelation. Also, at lower pH, H^+ ions were adsorbed onto the surface of Fe_3O_4 leading to a net positive charge. Thus, it can be envisaged that there is no adsorption of metal ions at pH < pH_{pzc}. However, in the present studies, a certain amount of metal ions were still adsorbed by carboxyl MNP at pH < pH_{pzc}. It is perhaps due to the fact that ion exchange takes effect at pH < pH_{pzc}. Since the affinity of metal ions to Fe_3O_4 is higher than that of H^+ ions, metal ions can replace the adsorbed

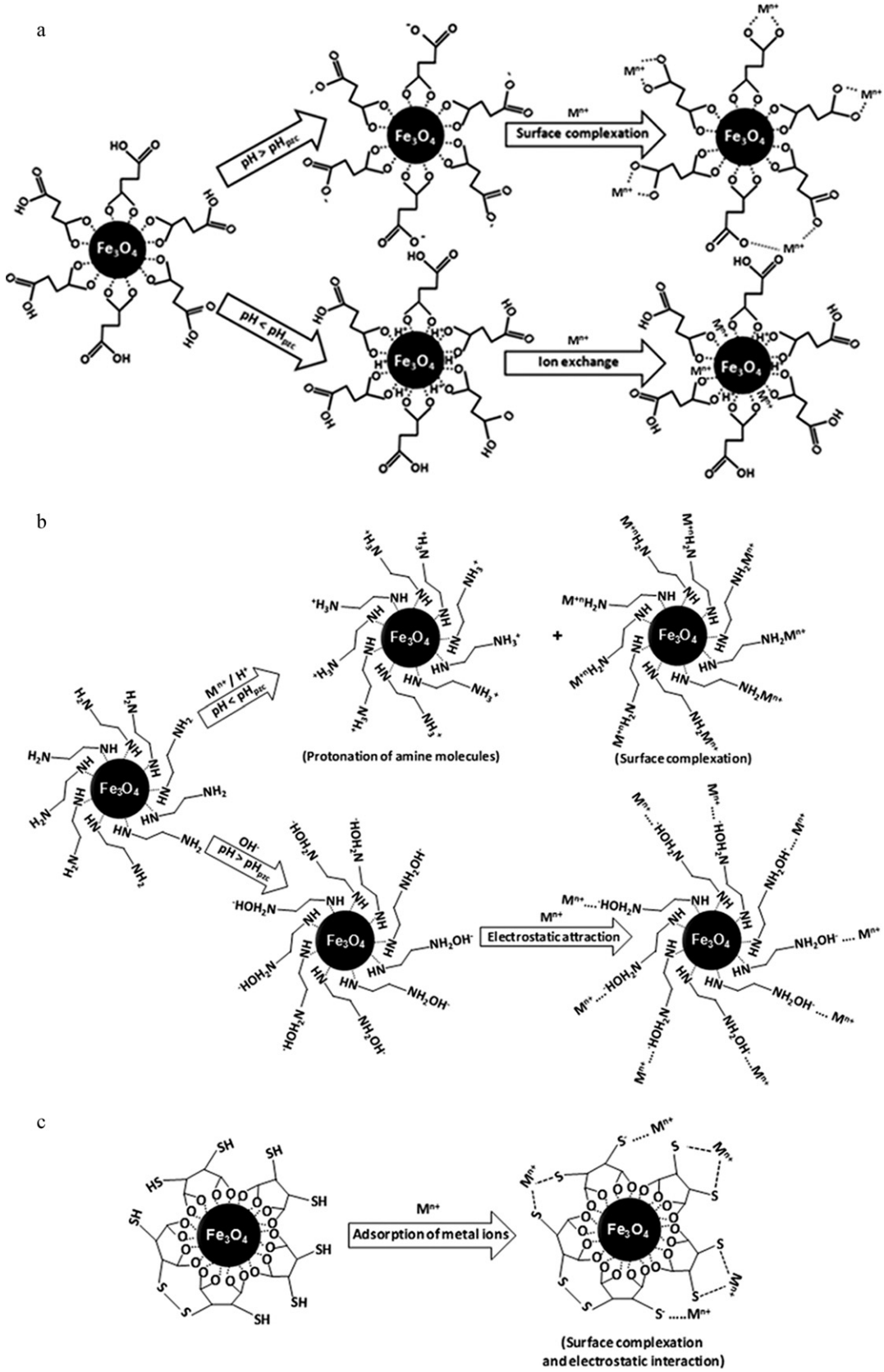

Scheme 1. The schematic representations of possible mechanism for adsorption of metal ions by (a) carboxyl MNP, (b) amine MNP and (c) thiol MNP.

H^+ ions from Fe_3O_4 surface by ion exchange mechanism [9]. Liu et al. [11] also observed that the adsorption of metal ions particularly Cd^{2+} took place directly on the surface of Fe_3O_4 rather than the coated organic moiety (humic acid). The adsorption of metal ions by ion exchange is relatively slower as compared to surface complexation since the organic molecules present on the surface of Fe_3O_4 may cause steric hindrance towards the adsorption of metal ions. The decrease in adsorption efficiency of As^{3+} at pH above 8 is

mainly due to the electrostatic repulsion among negatively charged AsO_3^{3-}/$As(OH)_4^-$ and negatively charged carboxyl MNP.

In case of amine MNP, the adsorption characteristics of metal ions with solution pH may be explained by Scheme 1(b), which depicts the major possible reactions that can take place at the solid–solution interface of amine MNP [28]. At $pH < pH_{pzc}$, the protonation of amine groups ($-NH_3^+$) and surface complexation of metal ions ($-NH_2M^{n+}$) may occur simultaneously on the surface of amine MNP. With the conversion of more $-NH_2$ groups to $-NH_3^+$, there were only fewer $-NH_2$ sites available on Fe_3O_4 surface for the adsorption of metal ions through complexation. Moreover, the electrostatic repulsion between M^{n+} and surfaces of Fe_3O_4 nanoparticles increased with the formation of more $-NH_3^+$. All these effects would result in the reduction of M^{n+} adsorption on amine MNP at low pH. On the other hand, the H^+ ion concentration decreases upon increasing the pH of solution (till pH_{pzc}) and hence, increases the free $-NH_2$ sites on Fe_3O_4 surface for the adsorption of metal ions through complexation. However, the surface of amine MNP is negatively charged at higher pH ($pH > pH_{pzc}$) possibly due to the formation of $-NH_2OH^-$. On one hand this could reduce the adsorption of metal ions through complexation, but on the other hand it might increase the adsorption of metal ions through the electrostatic attraction between the NH_2OH^- and M^{n+}. Thus, the ability of metal ions separation increases with increasing pH of the solution (NH_2OH^- sites increases) which leads to almost 100% removal of all analyzed metal ions (except As^{3+}).

As anticipated from Pearson's hard soft acid-base theory (HSAB) [29], the soft Lewis base such as thiol (—SH) group would be more favorable to undergo remarkable interaction with soft Lewis acids (heavy metal ions) rather than hard Lewis acids (alkali and alkaline earth metal ions). Thus, the thiol group (containing soft donor atom, sulfur) on the surface of MNP mainly reacts with heavy metal ions directly to form stable metal–sulfur complexes through chelation [21,30]. In addition to the metal–sulfur complexation, Liang et al. [31] reported the non-specific adsorption of metal ions by thiol functionalized silica nanoparticles through less selective electrostatic interaction between the metal ions and the oppositely charged surface functional groups at a certain distance from the surface. Thus, in case of thiol MNP, the adsorption mechanism of metal ions may involve two surface reactions namely strong metal–sulfur complexation and weak electrostatic interaction as depicted in Scheme 1(C). Most of the toxic metal ions investigated in the present study (except As^{3+}) were almost 100% adsorbed onto the surface of thiol MNP at pH 8 and above, whereas the same was observed at pH 10 and above in carboxyl MNP and amine MNP. This implies a higher adsorption affinity of metal ions towards thiol MNP.

The adsorption kinetic studies were performed with amine MNP to determine the effect of contact time on adsorption processes. The adsorption kinetic studies reveal two-stage adsorption behavior, a very rapid initial adsorption, followed by longer period of considerably slower uptake (Fig. S5 of Supplementary data shows a typical adsorption kinetic plot of amine MNP). It is apparent that the adsorption of metal ions onto surface of MNP is a fast process and most of the adsorption happened in a short period (<15 min) and the system achieved pseudo equilibrium at 60 min of contact time from the commencement of adsorption process. Rapid adsorption may be attributed to higher density of reactive sites (functional groups) on the particle surfaces, large surface area of particles, and/or higher intrinsic reactivity of the surface sites. Similar results were also observed for carboxyl and thiol MNP. The short equilibrium time needed suggests that these surface engineered magnetic nanoparticles have high adsorption efficiency to the removal of toxic metal ions from water, which would be helpful in lowering the capital and operational costs for industrial applications. Fig. 5 shows (a) desorption ratio of adsorbed toxic metal ions

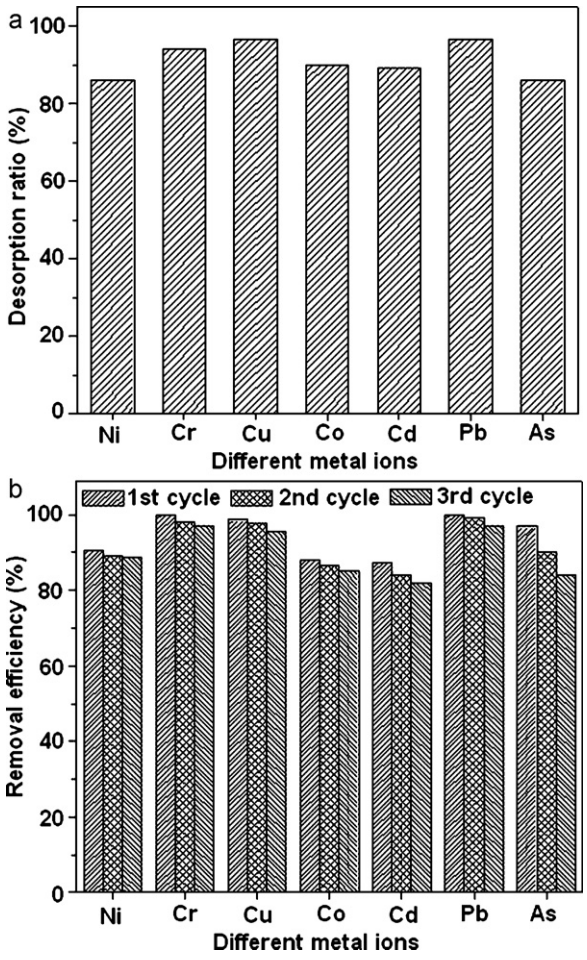

Fig. 5. (a) Desorption ratio of adsorbed toxic metal ions (after first adsorption–desorption cycle) using 10 ml of 0.1 M HCl and (b) removal efficiency of toxic metal ions during three different adsorption cycles by amine MNP at pH 8.

(after first adsorption–desorption cycle) using 10 ml of 0.1 M HCl and (b) removal efficiency of toxic metal ions during three different adsorption cycles by amine MNP at pH 8. All the metal ions showed over 85% of desorption ratio in their first adsorption–desorption cycle (Fig. 5(a)). Furthermore, it has been observed that the removal efficiency of metal ions is reduced gradually in the later cycles (Fig. 5(b)); however the removal efficiency of all metal ions investigated in the present study is still above 80% after three cycles. The gradual decrease in the removal efficiency could be attributed to incomplete release of adsorbed metal ions. Another reason for incomplete desorption of metal ions could be the dilute concentration of used HCl. The functional groups present on the surface of MNP need to be protonated for desorption of adsorbed toxic metal ions. However, to avoid the dissolution of magnetic nanoadsorbents, 0.1 M HCl concentration was preferred. This reusability of adsorbent is one of the most important features for their promising applications in environmental detoxification.

3.4. Capturing of bacterial pathogens by surface engineered magnetic nanoparticles

Fig. 6 shows the capture efficiency of *E. coli* by carboxyl MNP, amine MNP and thiol MNP after 12 h inoculation. It has been observed that the capture efficiency of bacterial pathogen is strongly dependent on the concentration of surface engineered MNP. Furthermore, capture efficiency significantly increases with

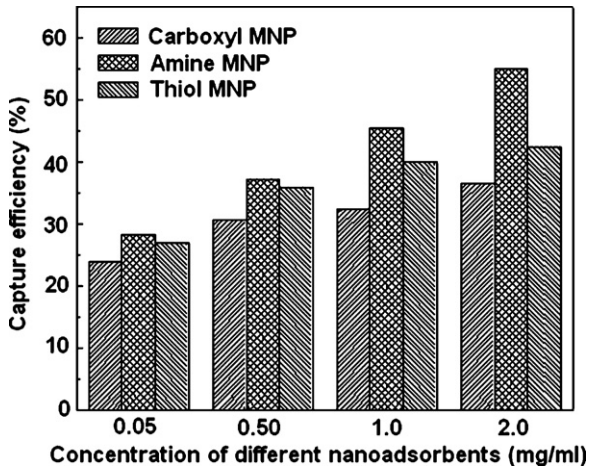

Fig. 6. Capture efficiency of *E. coli* by carboxyl MNP, amine MNP and thiol MNP after 24 h inoculation.

increasing the inoculation time from 12 h to 24 h (Fig. S6 of Supplementary data). These results indicate that surface engineered MNP possessed excellent capture performance to *E. coli* and well matched with the earlier reports on concentration and time dependent bacterial inhibition by nanoparticles [32]. The SEM-EDS elemental analysis and Kα spectral mapping of MNP treated *E. coli* (*E. coli* obtained after incubating these bacteria with MNP) showed that nanoparticles (nanoparticles were not visible due to the lower magnification of SEM images) were adsorbed/incorporated to the membrane of the treated bacterial cells (Fig. S7 of Supplementary data).

In order to investigate the cause of surface engineered MNP to be bactericidal, we have further studied the TEM analysis of *E. coli* (control) and carboxyl MNP treated *E. coli*. From the TEM images (Fig. 7), it has been observed that bacterial pathogens are successfully trapped by MNP (particles bind to spots on the surface of the *E. coli* rather than entire surface). The cell wall of the bacteria trapped by the magnetic nanoparticles is almost damaged whereas that of control bacteria (i.e., not exposed to MNP) is intact. Furthermore, it is clearly observed that nanoparticles partially/completely penetrate into the lipid bilayer component of the membrane and disrupts its structural integrity. This indicates the interaction of hydrophilic MNP with bacteria (possibly with the polar heads of membrane lipids) causes depolarization of the membrane which leads to cellular death. Recently, Lee et al. [33] reported the inactivation of *E. coli* by zero-valent iron nanoparticles due to the penetration of the small particles (sizes ranging from 10 to 80 nm) into *E. coli* membranes. Bromberg et al. [34] observed that poly(hexamethylene biguanide) modified magnetite and metallic cobalt-based nanoparticles kill bacteria (*E. coli*) on contact (nanoparticles cover entire surface of bacteria) due to the strong association with their membranes. Gu et al. [35] observed that the defects on the outer membrane of *E. coli* cause the binding of vancomycin functionalized magnetic (FePt) nanoparticles to *E. coli*. Basing on our bacteria-particle binding results (distribution of MNP on the surface of bacteria) and previous studies, it may be proposed that the smaller size surface functionalized magnetic nanoparticles capture bacterial pathogens on contact with cell wall and eventually kill them by disruption of the cell wall. The higher capture efficiency of *E. coli* by amine MNP as compared to carboxyl MNP and thiol MNP indicates that the surface functionality also plays crucial role in inhibition of bacterial growth. The present investigation suggested that surface functionalized magnetic nanoparticles may be used for capturing bacterial pathogens in the presence of appropriate external magnetic field. The main advantage of using more MNP for capture was a significant reduction in separation time. It is worth mentioning that in all the samples no residual adsorbents (Fe_3O_4) were observed in wastewater after capturing of toxic metal ions and bacterial pathogens. This is another important characteristic of magnetic separation techniques.

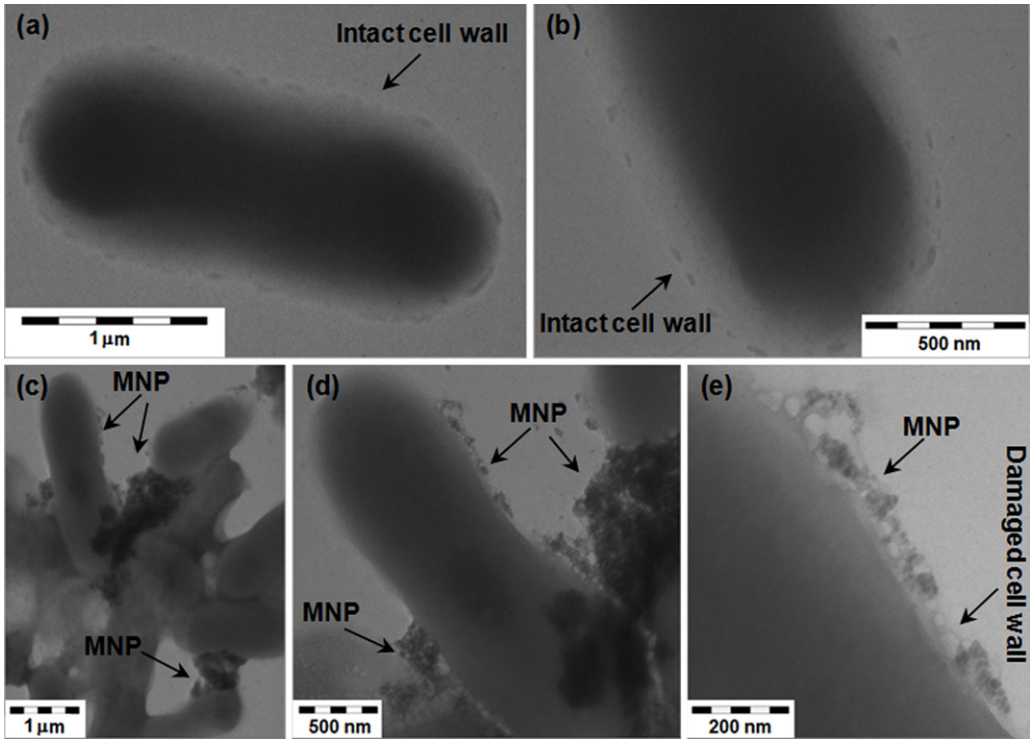

Fig. 7. TEM images of (a and b) *E. coli* (control) and (c–e) *E. coli* obtained after incubating these bacteria with carboxyl MNP.

4. Conclusion

Superparamagnetic carboxyl, amine and thiol functionalized Fe_3O_4 nanoparticles were synthesized by facile soft-chemical approaches. The structural analyses confirmed the formation of single-phase inverse spinel Fe_3O_4 nanoparticles and their functionalization with respective organic molecules. It has been observed that these surface engineered magnetic nanoparticles have strong affinity for the simultaneous adsorption of Cr^{3+}, Co^{2+}, Ni^{2+}, Cu^{2+}, Cd^{2+}, Pb^{2+} and As^{3+} from waste-water. The adsorption process was found to be highly dependent on the surface functionality of Fe_3O_4 and pH of the medium which made the nanoparticles selectively adsorb metal ions. More specifically, our results suggest that these surface engineered magnetic nanoparticles are highly effective, efficient and economically viable magnetic nanoadsorbents for the removal of toxic metal ions and bacterial pathogens from water in comparison to the existing industrial purification processes. Furthermore, these magnetic nanoadsorbents may be separated easily from the solution with the help of an external magnetic force and are reusable after removing the adsorbed toxic contaminants.

Acknowledgements

The financial support by nanomission of DST, Govt. of India is gratefully acknowledged. Sarika Singh acknowledges CSIR, India for the award of Junior Research Fellowship (JRF).

Appendix A. Supplementary data

Supplementary data associated with this article can be found, in the online version, at doi:10.1016/j.jhazmat.2011.06.074.

References

[1] L. Zhou, Y. Wang, Z. Liu, Q. Huang, Characteristics of equilibrium, kinetics studies for adsorption of Hg(II), Cu(II) and Ni(II) ions by thiourea-modified magnetic chitosan microspheres , J. Hazard. Mater. 161 (2009) 995–1002.
[2] Y.-T. Zhou, H.-L. Nie, C. Branford-White, Z.-Y. He, L.-M. Zhu, Removal of Cu^{2+} from aqueous solution by chitosan-coated magnetic nanoparticles modified with α-ketoglutaric acid , J. Colloid Interface Sci. 330 (2009) 29–37.
[3] S. Chen, Y. Zou, Z. Yan, W. Shen, S. Shi, X. Zhang, H. Wang, Carboxymethylated-bacterial cellulose for copper and lead ion removal , J. Hazard. Mater. 161 (2009) 1355–1359.
[4] Y. Chen, B. Pan, H. Li, W. Zhang, L. Lv, J. Wu, Selective removal of Cu(II) Ions by using cation-exchange resin-supported polyethyleneimine (PEI) nanoclusters , Environ. Sci. Technol. 44 (2010) 3508–3513.
[5] V. Ivanov, J.H. Tay, S.T. Tay, H.L. Jiang, Removal of micro-particles by microbial granules used for aerobic wastewater treatment , Water Sci. Technol. 50 (2004) 147–154.
[6] Z. Yong-Gang, S. Hao-Yu, P. Sheng-Dong, H. Mei-Qin, Synthesis, characterization and properties of ethylenediamine-functionalized Fe_3O_4 magnetic polymers for removal of Cr(VI) in wastewater , J. Hazard. Mater. 182 (2010) 295–302.
[7] S.M. Maliyekkal, K.P. Lisha, T. Pradeep, A novel cellulose-manganese oxide hybrid material by in situ soft chemical synthesis and its application for the removal of Pb(II) from water , J. Hazard. Mater. 181 (2010) 986–995.
[8] A.L. Buttice, J.M. Stroot, D.V. Lim, P.G. Stroot, N.A. Alcantar, Removal of sediment and bacteria from water using green chemistry , Environ. Sci. Technol. 44 (2010) 3514–3519.
[9] Y.F. Shen, J. Tang, Z.H. Nie, Y.D. Wang, Y. Ren, L. Zuo, Preparation and application of magnetic Fe_3O_4 nanoparticles for wastewater purification , Sep. Purif. Technol. 68 (2009) 312–319.
[10] Y.F. Shen, J. Tang, Z.H. Nie, Y.D. Wang, Y. Ren, L. Zuo, Tailoring size and structural distortion of Fe_3O_4 nanoparticles for the purification of contaminated water , Bioresour. Technol. 100 (2009) 4139–4146.
[11] J.F. Liu, Z.S. Zhao, G.B. Jiang, Coating Fe_3O_4 magnetic nanoparticles with humic acid for high efficient removal of heavy metals in water , Environ. Sci. Technol. 42 (2008) 6949–6954.
[12] L. Zhong, J. Hu, H. Liang, A. Cao, W. Song, L. Wan, Self-assembled 3D flowerlike iron oxide nanostructures and their application in water treatment , Adv. Mater. 18 (2006) 2426–2431.
[13] R.D. Ambashta, M. Sillanpää, Water purification using magnetic assistance: a review , J. Hazard. Mater. 180 (2010) 38–49.
[14] J.-C. Liu, P.-J. Tsai, Y.C. Lee, Y.-C. Chen, Affinity capture of uropathogenic *Escherichia coli* using pigeon ovalbumin-bound Fe_3O_4@Al_2O_3 magnetic nanoparticles , Anal. Chem. 80 (2008) 5425–5432.
[15] L.-H. Liu, H. Dietsch, P. Schurtenberger, M.-D. Yan, Photoinitiated coupling of unmodified monosaccharides to iron oxide nanoparticles for sensing proteins and bacteria , Bioconjugate Chem. 20 (2009) 1349–1355.
[16] K.C. Barick, M. Aslam, Y.-P. Lin, D. Bahadur, P.V. Prasad, V.P. Dravid, Novel and efficient MR active aqueous colloidal Fe_3O_4 nanoassemblies , J. Mater. Chem. 19 (2009) 7023–7029.
[17] S. Laurent, D. Forge, M. Port, A. Roch, C. Robic, L.V. Elst, R.N. Muller, Magnetic iron oxide nanoparticles: synthesis, stabilization, vectorization, physicochemical characterizations, and biological applications , Chem. Rev. 108 (2008) 2064–2110.
[18] Z. Liu, J. Ding, J. Xue, A new family of biocompatible and stable magnetic nanoparticles: silica cross-linked pluronic F127 micelles loaded with iron oxides , New J. Chem. 33 (2009) 88–92.
[19] S. Chandra, S. Mehta, S. Nigam, D. Bahadur, Dendritic magnetite nanocarriers for drug delivery applications , New J. Chem. 34 (2010) 648–655.
[20] X. Liu, Q. Hu, Z. Fang, X. Zhang, B. Zhang, Magnetic chitosan nanocomposites: a useful recyclable tool for heavy metal ion removal , Langmuir 25 (2009) 3–8.
[21] W. Yantasee, C.L. Warner, T. Sangvanich, R. Shaneaddleman, T.G. Carter, R.J. Wiacek, G.E. Faryxell, C.T. Timchalk, M.G. Warner, Removal of heavy metals from aqueous systems with thiol functionalized superparamagnetic nanoparticles , Environ. Sci. Technol. 41 (2007) 5114–5119.
[22] K.C. Barick, M. Aslam, P.V. Prasad, V.P. Dravid, D. Bahadur, Nanoscale assembly of amine functionalized colloidal iron oxide , J. Magn. Magn. Mater. 321 (2009) 1529–1532.
[23] S. Nigam, K.C. Barick, D. Bahadur, Development of citrate-stabilized Fe_3O_4 nanoparticles: conjugation and release of doxorubicin for therapeutic applications , J. Magn. Magn. Mater. 323 (2011) 237–243.
[24] Y. Jun, Y.-M. Huh, J. Choi, J.-H. Lee, H.-T. Song, S. Kim, S. Yoon, K.-S. Kim, J.-S. Shin, J.-S. Suh, J. Cheon, Nanoscale size effect of magnetic nanocrystals and their utilization for cancer diagnosis via magnetic resonance imaging , J. Am. Chem. Soc. 127 (2005) 5732–5733.
[25] Y.-C. Chang, D.-H. Chen, Preparation and adsorption properties of monodisperse chitosan-bound Fe_3O_4 magnetic nanoparticles for removal of Cu(II) ions , J. Colloid Interface Sci. 283 (2005) 446–451.
[26] K.C. Barick, D. Bahadur, Assembly of Fe_3O_4 nanoparticles on SiO_2 monodisperse spheres , Bull. Mater. Sci. 29 (2006) 595–598.
[27] K.E. Engates, H.J. Shipley, Adsorption of Pb, Cd, Cu, Zn, and Ni to titanium dioxide nanoparticles: effect of particle size, solid concentration, and exhaustion , Environ. Sci. Pollut. Res. 18 (2011) 386–395.
[28] S.S. Banerjee, D.-H. Chen, Fast removal of copper ions by gum Arabic modified magnetic nano-adsorbent , J. Hazard. Mater. 147 (2007) 792–799.
[29] R.G. Pearson, Hard and soft acids and bases , J. Am. Chem. Soc. 85 (1963) 3533–3539.
[30] Q. Zhang, B. Pan, W. Zhang, B. Pan, L. Lv, X. Wang, J. Wu, X. Tao, Selective removal of Pb(II), Cd(II), and Zn(II) ions from waters by an inorganic exchanger $Zr(HPO_3S)_2$, J. Hazard. Mater. 170 (2009) 824–828.
[31] X. Liang, Y. Xu, G. Sun, L. Wang, Y. Sun, X. Qin, Preparation, characterization of thiol-functionalized silica and application for sorption of Pb^{2+} and Cd^{2+} , Colloids Surf., A 349 (2009) 61–68.
[32] N. Tran, A. Mir, D. Mallik, A. Sinha, S. Nayar, T. Webster, Bactericidal effect of iron oxide nanoparticles on *Staphylococcus aureus* , Intern. J. Nanomed. 5 (2010) 277–283.
[33] C. Lee, J.Y. Kim, W.I. Lee, K.L. Nelson, J. Yoon, D.L. Sedlak, Bactericidal effect of zero-valent iron nanoparticles on *Escherichia coli* , Environ. Technol. 42 (2008) 4927–4933.
[34] L. Bromberg, E.P. Chang, C. Alvarez-Lorenzo, B. Magariños, A. Concheiro, T.A. Hatton, Binding of functionalized paramagnetic nanoparticles to bacterial lipopolysaccharides and DNA , Langmuir 26 (2010) 8829–8835.
[35] H. Gu, K. Xu, C. Xu, B. Xu, Biofunctional magnetic nanoparticles for protein separation and pathogen detection , Chem. Commun. 94 (2006) 1–949.